ACS APPLIED MATERIALS & INTERFACES

www.acsami.org

Research Article

Split-Type Electrochemical Immunoassay System Triggering Ascorbic Acid-Mediated Signal Magnification Based on a Controlled-Release Strategy

Liu Qu, Xiang Ren, Dawei Fan, Xuan Kuang, Xu Sun, Bin Wang, Qin Wei,* and Huangxian Ju

Cite This: *ACS Appl. Mater. Interfaces* 2021, 13, 29179−29186

Read Online

ACCESS | Metrics & More | Article Recommendations | Supporting Information

ABSTRACT: This research put forward a novel split-type electrochemical (EC) immunosensor which integrated the controlled-release strategy with EC detection for application in the field of biosensing. Concretely, ascorbic acid (AA) was packaged in a cadmium sulfide (CdS)-capped spherical mesoporous bioactive glass (SBG) nanocarrier (SBG_{CdS}) on account of encapsulation technology. To reduce the complexity of the bioanalysis, the detection antibody-labeled SBG_{CdS}−AA bioconjugate was applied in a 96-well microplate for the immunoreaction process, which is independent of the EC determination procedure. Thus, the immune interference and steric hindrance caused by the accumulation of nanomaterials on the electrode could be minimized. Subsequently, AA was released efficiently via the destruction effect of dithiothreitol on the disulfide bond. In addition, for the as-prepared FcAl/L-Cys/gold nanoparticles (GNPs)/porous $BiVO_4$ (p-BVO)/ITO EC sensing platform in the detection solution, the synergetic catalysis of Fc and GNPs/p-BVO toward the oxidation of the released AA could be realized, which triggered AA-mediated significant signal magnification throughout this study. In particular, p-BVO with an ordered nanoarray structure could accelerate the electron transfer to assist in sensitivity improvement of this system. This novel biosensor was capable of assaying the neuron-specific enolase (NSE) biomarker sensitively, from which a linear range of 0.001−100 ng/mL was derived along with a low detection limit of 1.08 pg/mL. An innovative way could be paved in the bioanalysis of NSE and other biomarkers.

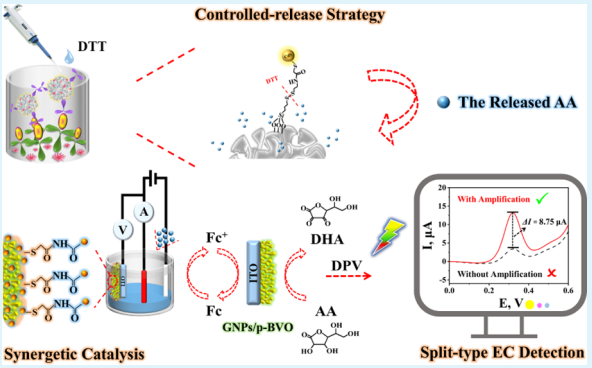

KEYWORDS: *controlled-release strategy, split-type EC immunosensor, SBG_{CdS}-AA, synergetic catalysis oxidation, neuron-specific enolase*

INTRODUCTION

Electrochemical (EC) immunoassay based on specific recognition of a target by the antibody is currently one of the most extensively explored assays.[1−3] Possessing merits of high sensitivity, wide dynamic response range, low background noise, and easy controllability, various types of EC strategies are put forward for trace-level disease markers analysis.[4−7] Nevertheless, the inherent defects of the traditional sandwich-type strategy are intricate operation and time consumption. Meanwhile, it should be highlighted that the accumulation of interference on the EC sensing platform caused by the immunoreaction process makes the traditional sandwich-type strategy unreliable for sensitive determination.[8] Therefore, a novel split-type immunoassay method has come into being and is highly demanded to overcome the abovementioned defects.[9] In particular, it separates the immunoreaction process from the EC detection platform, which could simplify the detection device and eliminate the impact of immune interference on the EC current signal.[10] From what has been discussed above, this novel method may exert its potential in creating more access for further immunoassays and biomedical applications.

For the split-type EC immunosensor that was constructed based on the controlled-release strategy, generally, a specific molecule or a nanomaterial was encapsulated into carrier materials to deliver the target substance.[11,12] Notably, the significant role that the carrier material played in this strategy could not be negligible. For instance, Wang et al.[13] proposed a gold nanoparticle (GNP)-capped cage fluorescent biosensor based on the controlled-release strategy for ultrasensitive detection of ATP; Xu et al.[14] designed a novel controlled-release system encapsulating ascorbic acid (AA) within a mesoporous silica nanosphere assisted by cadmium sulfide (CdS) caps. With reference to the abovementioned strategy, stable mesoporous nanomaterials with a multi-channel

Received: April 27, 2021
Accepted: May 27, 2021
Published: June 8, 2021

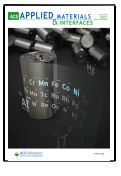

https://doi.org/10.1021/acsami.1c07780
ACS Appl. Mater. Interfaces 2021, 13, 29179−29186

Scheme 1. Fabrication Process of the EC Sensing Interface and the Signal-Amplification Mechanism of the Split-Type System[a]

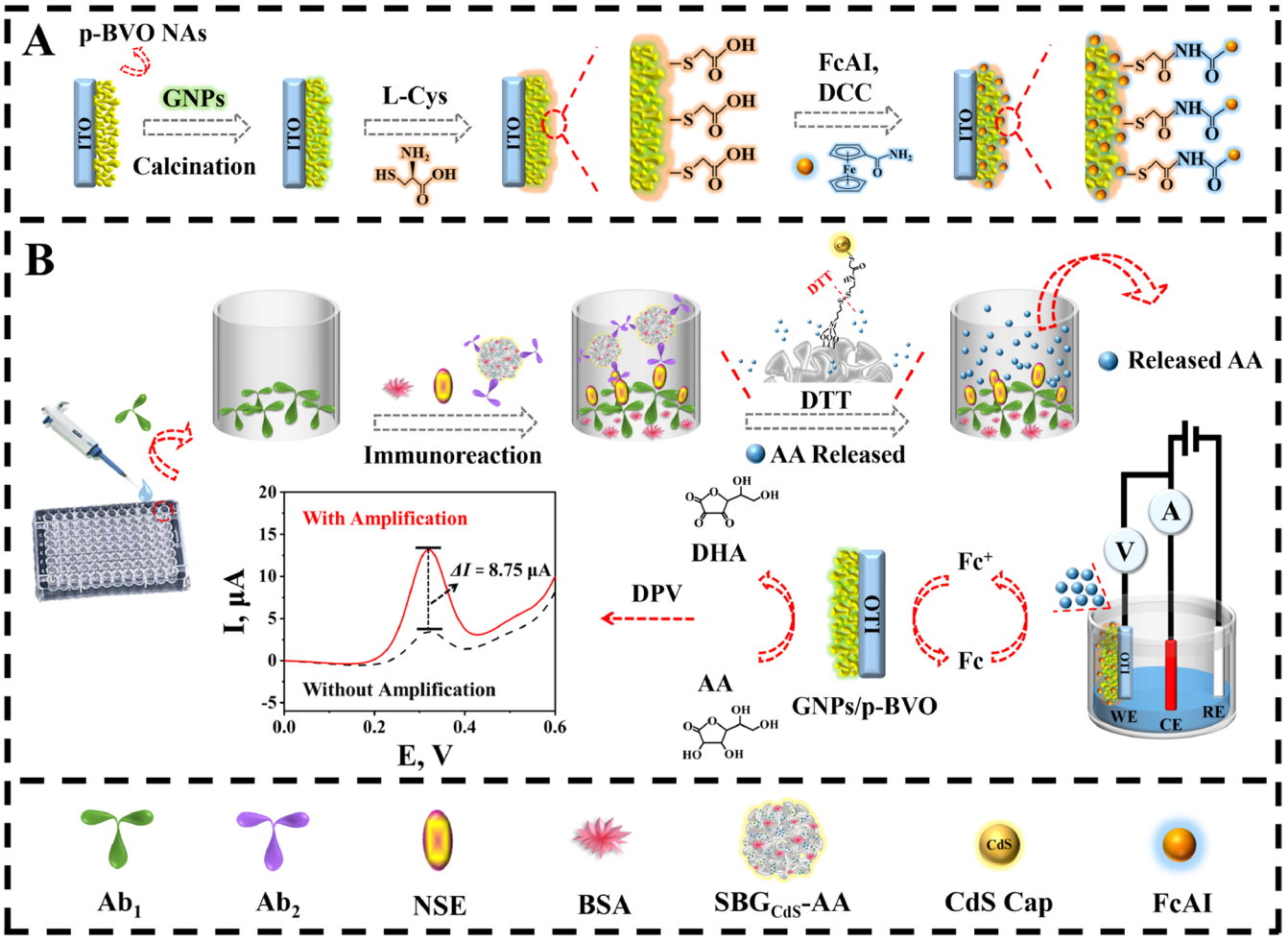

[a](A) Assembly process of the FcAI/L-Cys/GNPs/p-BVO/ITO EC sensing interface. (B) Detailed immunoassay procedure of the split-type system and comparative DPV signals with and without synergetic amplification.

structure and well-defined surface properties are the first choice of carriers. Spherical mesoporous bioactive glasses (SBGs) with uniform corrosive pores prepared by the sacrificial liquid template method has attracted widespread attention for its better biocompatibility.[15,16] Meanwhile, the tunable pore sizes and volumes, superior specific surface area, and stability endow it with possibility to be used as an ideal carrier for a controlled-release delivery system.[17] For packaging materials that encapsulate and release target molecules efficiently, CdS nanomaterials instead of single-stranded DNA or RNA aptamers would be a promising choice.[18] On one hand, the disulfide linkages could be easily cleaved through the dithiothreitol (DTT) reducing agent to simplify the operation process. On the other hand, using a CdS-capped SBG (SBG_{CdS}) system could reduce the cost to a certain extent.

Ferrocene (Fc) as a universally accepted redox probe exhibits outstanding EC activity. Simultaneously, the unique catalytic oxidation properties of Fc toward AA endow it with wide application in a variety of signal-amplification strategies.[19] In addition, GNPs could also act as a nanocatalyst to assist in AA oxidation.[20−22] Inspired by above reasonable findings, AA was effectively encapsulated in 2-(propyldisulfanyl)ethylamine-functionalized SBG nanocarriers which utilized the mercaptoacetic acid (MPA)-functionalized CdS as the cap, forming the SBG_{CdS}−AA conjugate for this study. Notably, this conjugate acted as a label to immobilize detection antibodies (Ab_2) for the immune recognition process. Simultaneously, an appropriate amount of packaged AA could be released from the SBG_{CdS}−AA signal probe in a timely manner by DTT, which effectively shortened the reaction time. Furthermore, aminylferrocene (FcAI) was immobilized through the *N*-*N*′-dicyclohexyl carbodiimide (DCC) coupling agent on L-cysteine (L-Cys)-modified GNP/porous $BiVO_4$ nanoarrays (p-BVO NAs), which could provide absolute loading capacity for Fc.[23] What is more, the electron transfer along the ordered nanoarray structure could accelerate the electrode reaction process for improvement of the sensitivity.[24] Consequently, FcAI/L-Cys/GNPs/p-BVO/ITO was designed as an EC sensing interface, and the signal-amplification approach is presented in detail (Scheme 1).[20]

Differing from the construction manner of the normal sandwich-type EC immunosensor, sandwich immunoassay based on the controlled-release strategy was carried out in a 96-well microplate. By this method, accumulation of nanomaterials and immune interference caused by antigen and antibody recognition were effectively avoided on the EC sensing interface. After the immunoreaction process, various amounts of released AA were transferred into the detection solution for EC detection. Subsequently, the synergetic

https://doi.org/10.1021/acsami.1c07780
ACS Appl. Mater. Interfaces 2021, 13, 29179−29186

catalysis of Fc and GNPs/p-BVO toward the oxidation of released AA could be realized, which led to a novel AA-mediated EC signal-amplification methodology. Strikingly, the proposed strategy was applied for neuron-specific enolase (NSE) real sample analysis, which acts as a reliable biomarker in early diagnosis of small-cell lung cancer.[25,26] This as-prepared strategy provided a good linearity ranging from 0.001 to 100 ng/mL with a low detection limit (LOD) determined as 1.08 pg/mL (S/N = 3). Consequently, accuracy and practicability of this immunosensor were well-verified in view of the above satisfying performance. To sum up, this work could open up a novel and efficient approach to combine the controlled-release strategy and EC detection for bioassay.

EXPERIMENTAL SECTION

Assembly Process of the FcAI/L-Cys/GNPs/p-BVO/ITO EC Sensing Interface. The preparation procedure of p-BVO/ITO was divided into two steps including electrodeposition and calcination according to our previous reports.[27,28] Subsequently, FcAI/L-Cys/GNPs/p-BVO/ITO was prepared by a three-step immersion method. The prepared p-BVO substrate was soaked in GNP solution for 12 h and washed and then dried at room temperature and calcined (350 °C, 1 h) to obtain GNPs/p-BVO/ITO. Then, L-Cys solution (10 mmol/L) was utilized to immerse the above electrode for 24 h, forming Au−S bonds through a strong chemical binding effect between the sulfhydryl group of the tail group of L-Cys and the GNPs to obtain L-Cys/GNPs/p-BVO/ITO.[8] Afterwards, the washed electrode was immersed in phosphate-buffered saline (PBS) solution (pH 7.4, containing 5 mmol/L FcAI and 10 mmol/L DCC) for 40 h; then, the final FcAI/L-Cys/GNPs/p-BVO/ITO EC sensing interface was obtained after washing with PBS solution[23] (Scheme 1A).

Preparation of SBG_{CdS}−AA. The preparation process of 2-(propyldisulfanyl)ethylamine-functionalized SBG and MPA-functionalized CdS is described in the Supporting Information. SBG_{CdS}−AA was prepared according to the work of Xu with some modification.[14] Primarily, 0.5000 g of AA was thoroughly mixed with 0.1000 g of 2-(propyldisulfanyl)ethylamine-functionalized SBG which was dissolved in 10 mL of PBS solution (pH 7.4) at room temperature. Subsequently, the obtained solution was stirred for 24 h. Next, 3 mL of MPA-functionalized CdS (4 mg/mL) and 0.0020 g of EDC were added into the above solution in turn. After another 24 h of stirring, the washed product was dried using the freeze-drying method to obtain SBG_{CdS}−AA.

Preparation of the SBG_{CdS}−AA−Ab_2 Bioconjugate. In brief, 1 mL of NSE Ab_2 (10 μg/mL), 20 μL of EDC/NHS solution (containing 5 mg/mL EDC and 1 mg/mL NHS), and 4 mL of the prepared SBG_{CdS}−AA-dispersed solution (2.5 mg/mL) were mixed thoroughly. Afterward, the mixture was shaken at 4 °C for 12 h followed by centrifugation and redispersed in 4 mL of PBS solution (pH 7.4). Finally, 0.0020 g of bovine serum albumin (BSA) was added to block nonspecific active sites of SBG_{CdS}−AA−Ab_2.

Immunoassay Procedure of the Split-Type System. Detailed immunoassay procedure of the split-type system is displayed in Scheme 1B. 100 μL of capture antibodies (Ab_1, 5 μg/mL) was initially injected into the 96-well microplate and incubated at 4 °C overnight. Next, the above microplate was incubated with 100 μL of BSA solution (0.1 wt %) at 4 °C for 1 h to prevent nonspecific adsorption. Subsequently, 100 μL of varying concentrations of NSE was dropped into the microplate and incubated at 37 °C for 1 h. Then, the prepared SBG_{CdS}−AA−Ab_2 bioconjugate was injected and incubated for another 1 h in the modified microplate. Notably, the 96-well microplate was washed with PBS solution (pH 7.4) after each modification procedure. Following that, 100 μL of DTT solution (2 mg/mL) was added to react with the above bioconjugate for 20 min to break the disulfide bond.[29,30] Eventually, the EC detection cell (containing 5 mL of PBS solution) was added with the released AA which was transferred from the above plate.

EC Measurements. Referring to the above split-type system, for the analysis of NSE, the prepared FcAI/L-Cys/GNPs/p-BVO/ITO acted as the working electrode to perform differential pulse voltammetry (DPV) measurements (voltage range: from 0 to 0.6 V) in the above PBS buffer solution (pH 7.4) which contained the released AA. Apparently, the detected DPV signal of the immunosensor was virtually associated to different concentrations of NSE.

ANALYSIS OF RESULTS

Characterization of Materials. To start with, X-ray diffraction (XRD) patterns (curves a and b) are utilized to characterize the lattice structure of BiOI nanosheets (BOI NSs) and p-BVO NAs (Figure 1A). As exhibited in curve a,

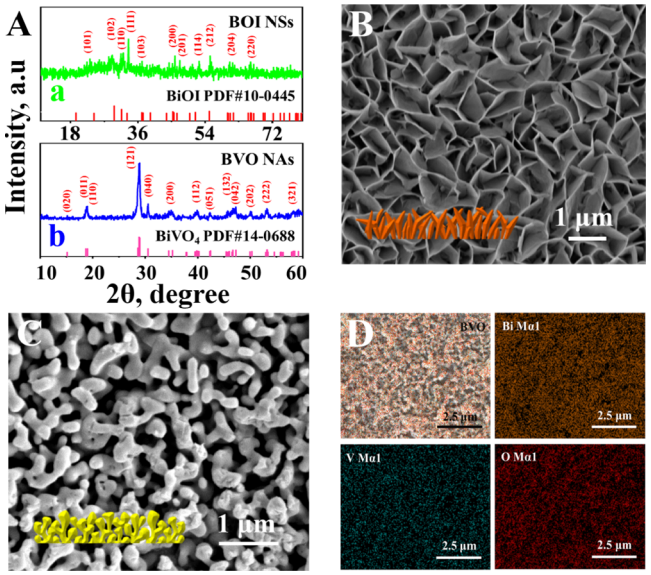

Figure 1. XRD patterns of BOI NSs and p-BVO NAs (A); SEM images of BOI NSs (B) and p-BVO NAs (C); and SEM mapping images depicting the elemental distribution of Bi, V, and O in p-BVO (D).

main diffraction peaks can be indexed to the tetragonal phase of BOI (JCPDS card no. 10-0445).[31] Diffraction peaks at 15.1, 28.9, 30.5, 34.5, 46.1, 47.3, 50.3, and 58.5° clearly correspond to the (020), (121), (040), (200), (042), (132), (202), and (321) planes, respectively, of scheelite-monoclinic p-BVO (JCPDS card no. 14-0688).[32] Figure 1B,C illustrates the scanning electron microscopy (SEM) images of BOI NSs and p-BVO NAs: it can be observed that large amounts of BOI NSs are distributed on the ITO surface in a certain arrangement (Figure 1B). Additionally, p-BVO in Figure 1C presents a coral-like shape. SEM elemental mapping images (Figure 1D) reveal the existence and relatively uniform distribution of elements of Bi, O, and V. The X-ray photoelectron spectroscopy (XPS) survey spectrum (Figure S1A−D) is applied to further demonstrate the existence and chemical state of components, which is described in detail in the Supporting Information. Figure S2A−C exhibits transmission electron microscopy (TEM) and high-resolution TEM (HRTEM) images, size distribution, and UV−vis spectra of the synthesized GNPs, respectively. It is observed from the SEM image of GNPs/p-BVO (Figure S3A) that GNPs were distributed on the surface of p-BVO. The SEM elemental mapping images and energy dispersive spectroscopy spectrum (Figure S3A,B) could further confirm the above view. In light

https://doi.org/10.1021/acsami.1c07780
ACS Appl. Mater. Interfaces 2021, 13, 29179−29186

of the above results, the synthesis of p-BVO NAs and GNPs/p-BVO is manifested to be successful.

Several characterization methods were also applied to demonstrate the successful preparation of SBG and SBG_{CdS}–AA. The SEM image and TEM image of SBG (Figure 2A,B)

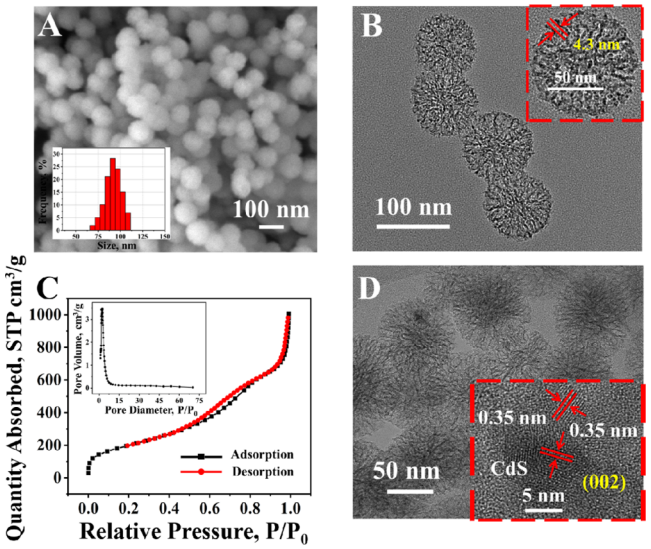

Figure 2. SEM image of SBG (A); TEM and enlarged TEM images of SBG (B); N_2 adsorption/desorption isotherm and pore-size distribution of SBG nanospheres (C); and TEM and HRTEM images of SBG_{CdS}–AA (D).

exhibit its regularly spherical morphology with the average size measured to be approximately 96.19 nm. As depicted in Figure 2B, the enlarged TEM image confirms that radial corrosive pores are distributed inside the spherical-like SBG with an average pore diameter of about 4.3 nm. The Brunauer–Emmett–Teller (BET) results (Figure 2C) of slit-shaped pores are consistent with above TEM results. Meanwhile, the outstanding specific surface area and total pore volume of SBG nanospheres are verified. The Fourier transform infrared spectroscopy (FTIR) spectrum is applied to verify the successful preparation of MPA-functionalized CdS (Figure S4, Supporting Information). The TEM image of SBG_{CdS}–AA (Figure 2D) exhibits that CdS caps are distributed on the surface of SBG. Furthermore, paralleled and ordered lattice fringes with a *d*-spacing of 0.35 nm are found (Figure 2D) in the HRTEM image region, which is well-consistent with the (002) face of CdS crystals. The element mapping image of SBG_{CdS}–AA prepared above is depicted in Figure S5 (Supporting Information), which clearly displays each of the element distribution.

EC Characterization and EIS Characterization. Herein, the assembly process of the FcAI/L-Cys/GNPs/p-BVO/ITO EC sensing interface was investigated using electrochemical impedance spectroscopy (EIS) and cyclic voltammetry (CV).[33] As depicted in Figure 3A, the Nyquist plots of EIS results were recorded in 5.0 mmol/L $[Fe(CN)_6]^{3-/4-}$ PBS solution (pH 7.4) containing 0.1 mol/L KCl. Compared with pure p-BVO/ITO (curve a), the impedance value of GNPs/p-BVO/ITO (curve b) is greatly reduced, which demonstrates the successful modification of GNPs, whereas L-Cys/GNPs/p-BVO/ITO (curve c) is noticed to exhibit a larger semicircle domain. This is because the L-Cys modification layer (isoelectric point 5.02) has a negative charge on its surface

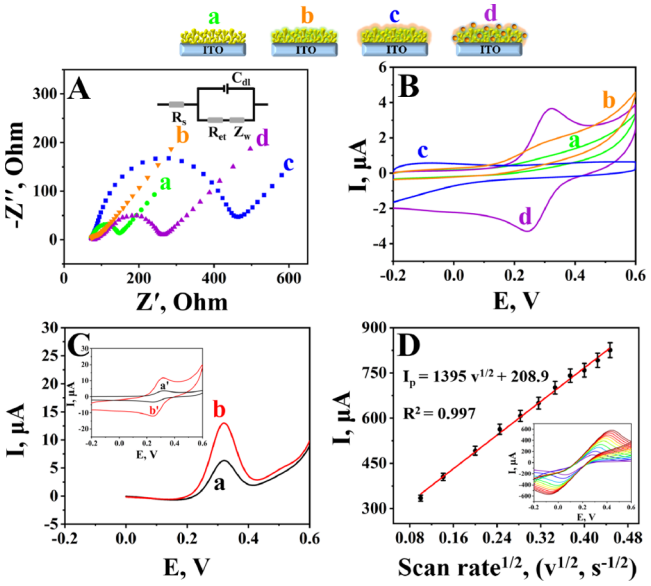

Figure 3. (A) Nyquist impedance plots and (B) CV responses of pure p-BVO/ITO (a), GNPs/p-BVO/ITO (b), L-Cys/GNPs/p-BVO/ITO (c), and FcAI/L-Cys/GNPs/p-BVO/ITO (d); (C) CV and DPV responses of FcAI/L-Cys/GNPs/p-BVO/ITO in PBS solution (a′, a) and in PBS solution containing the released AA from the 96-well plate (b′, b, c_{NSE} = 0.05 ng/mL); and (D) CV responses for determining the electroactive surface area at different scan rates (inset) and the linear relation between I_p and scan rate$^{1/2}$.

in the above test solution, which is repellent to the $[Fe(CN)_6]^{4-/3-}$ probe, thus hindering the charge transfer. Consequently, the impedance of L-Cys/GNPs/p-BVO/ITO (curve c) increased significantly. Nevertheless, after FcAI was bonded, $[Fe(CN)_6]^{4-/3-}$ was attracted to positively charged Fc^+ during the electrode reaction, making it easy to reach the modified electrode surface. Thus, it could be observed that the impedance value of FcAI/L-Cys/GNPs/p-BVO/ITO (curve d) got weaker as compared to that of L-Cys/GNPs/p-BVO/ITO (curve c). The above EIS results highlighted the successful assembly process of the FcAI/L-Cys/GNPs/p-BVO/ITO EC sensing interface.

CV tested in PBS buffer solution (pH 7.4) was applied for further verifying the above construction steps of the interface. As can be seen, the CV curves illustrated in Figure 3B are in good agreement with the EIS result. Especially, a pair of well-defined redox peaks (assigned to the signal of Fc) in the curve c were observed in the range of 0.2–0.4 V, indicating that the FcAI/L-Cys/GNPs/p-BVO/ITO EC sensing interface was assembled successfully. Additionally, the CV method was also adopted to detect the increased electroactive surface area of p-BVO NAs (Figure 3D). The specific analysis procedure which is described in the Supporting Information was carried out with reference to the Randles–Sevcik equation.[34]

$$I_p = 2.69 \times 10^5 n^{3/2} D^{1/2} v^{1/2} AC \quad (1)$$

$$A = k/(2.69 \times 10^5 n^{3/2} D_0^{1/2} C_0) \quad (2)$$

EC Performance Comparison of the CV and DPV Method. It is worth mentioning that the CV and DPV method were applied for studying the compared EC performance of the split-type immunosensor. As illustrated in Figure 3C, it could be clearly observed that both the CV and DPV current response (curve b and b′) of the immunosensor

https://doi.org/10.1021/acsami.1c07780
ACS Appl. Mater. Interfaces 2021, 13, 29179–29186

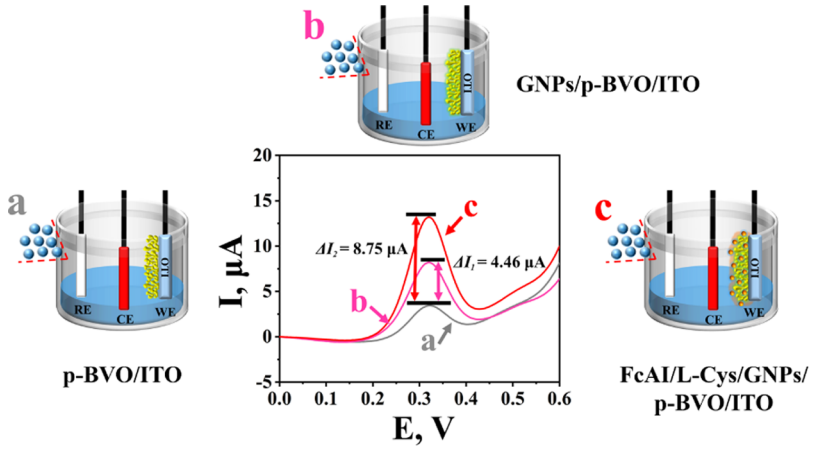

Figure 4. DPV responses of the three modified electrodes (with AA): p-BVO/ITO (a), GNPs/p-BVO/ITO (b), and FcAI/L-Cys/GNPs/p-BVO/ITO (c) to investigate the synergistic catalytic oxidation mechanism.

increased after the released AA from the 96-well microplate was transferred into the PBS testing solution, whereas a remarkable amplification of DPV current response (Figure 3C) was further noticed in comparison with the CV result (Figure 3C, inset). In view of the above results, the DPV method with superior performance was applied in the EC analysis process of NSE in this work.

Mechanism of Synergistic Catalytic Oxidation of AA. To explore the synergistic catalytic oxidation mechanism of FcAI and GNPs/p-BVO (FcAI/L-Cys/GNPs/p-BVO/ITO), the contrast experiment to compare DPV responses of the EC sensing interface in three modified states was investigated. The abovementioned immunosensors were all incubated with 0.05 ng/mL NSE and the released AA was transferred to the detecting solution. As depicted in Figure 4, the DPV response of GNPs/p-BVO/ITO (curve b) increased by around 4.46 μA compared with that of p-BVO/ITO (curve a), indicating the excellent catalytic oxidation effect of GNPs/p-BVO on AA. Subsequently, about 8.75 μA higher DPV response was obtained with FcAI/L-Cys/GNPs/p-BVO/ITO (curve c). In light of above results, the signal amplification could be ascribed to the synergistic catalytic oxidation mechanism of FcAI and GNPs/p-BVO toward AA.

Experimental Condition Optimization Test. For the purpose of realizing sensitive analysis of NSE under best EC performance, the choice of optimal experimental conditions is of great significance. First, given that the pH environment of the PBS electrolyte could affect the performance of the bioanalysis system, the pH values of PBS were evaluated.[35] As depicted in Figure S6A, pH 7.4 was observed to be the most suitable for further investigation. Moreover, the effect of the concentration of the SBG_{CdS}–AA label on the sensing system was investigated, and it is shown in Figure S6B. Apparently, the tested I_p achieved the maximum value at 2.5 mg/mL SBG_{CdS}–AA, whereas the signal response tended to decrease as the concentration of the label continued to increase. Thus, 2.5 mg/mL was selected as the optimal concentration of SBG_{CdS}–AA. Notably, DTT reaction time is the key to influence the released AA so it would affect the EC performance greatly. As illustrated in Figure S6C, I_p reached a peak while the reaction time came to 20 min, which might indicate that the released AA was at its maximum. Therefore, the DTT reaction time was optimized to 20 min. In addition, the effect of soaking time of p-BVO/ITO on GNPs is exhibited in Figure S6D (Supporting Information), and 12 h was regarded as the optimal soaking time.

EC Detection for NSE. By virtue of the proposed split-type system that separated the immunoreaction process from the EC detection process,[8] herein, a series of concentration gradients of NSE were evaluated under optimal experimental conditions. As depicted in Figure 5A, the DPV signal exhibited

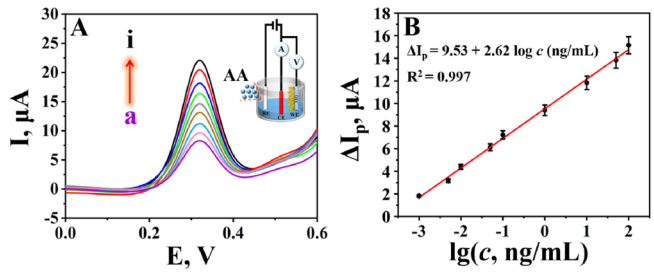

Figure 5. (A) DPV responses of the proposed split-type EC immunosensor with NSE at various concentrations (a–i) 0.001, 0.005, 0.01, 0.05, 0.1, 1, 10, 50, and 100 ng/mL, respectively and (B) calibration curves of the immunosensor based on ΔI_p as the response signal toward NSE detection at different logarithm of concentrations. Error bars = standard deviation (SD) (n = 5).

an upward trend with enhancement in the concentration of NSE. Meanwhile, a good linear correlation between ΔI_p ($\Delta I_p = I_{pa} - I_{pb}$, where I_{pb} and I_{pa} are peak currents of the modified EC sensing interface before and after amplified by the released AA) and the logarithm of NSE concentration from 0.001 to 100 ng/mL is shown in Figure 5B. The regression equation is $\Delta I_p = 9.53 + 2.62 \log c_{NSE}$ (ng/mL) with a correlation coefficient (R^2) of 0.997. Furthermore, the LOD was calculated to be 1.08 pg/mL (S/N = 3). Notably, a superior EC analytical performance in this work was made in comparison with other reported detection methods (Table S2, Supporting Information).

Performance Analysis of the Proposed Immunosensor. The reproducibility of this proposed immunosensor has been evaluated with seven electrodes for detecting 0.05 ng/mL NSE, which exhibited a relative standard deviation (RSD) of less than 5%. As illustrated in Figure 6A, the result indicated the acceptable reproducibility of this immunosensor.

It should be noted that selectivity is recognized as the paramount assessment for immunosensor performance in real

https://doi.org/10.1021/acsami.1c07780
ACS Appl. Mater. Interfaces 2021, 13, 29179–29186

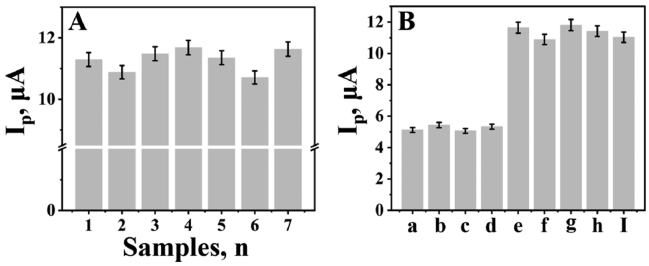

Figure 6. (A) Reproducibility test of the proposed immunosensor with seven electrodes for the detection of NSE (c_{NSE} = 0.05 ng/mL) and (B) DPV responses of FcAI/L-Cys/GNPs/p-BVO/ITO toward 5 ng/mL AFP (a), 5 ng/mL PSA (b), 5 ng/mL BNP (c), 5 ng/mL cTnI (d), 0.05 ng/mL NSE (e), 0.05 ng/mL NSE + 5 ng/mL AFP (f), 0.05 ng/mL NSE + 5 ng/mL PSA (g), 0.05 ng/mL NSE + 5 ng/mL BNP (h), and 0.05 ng/mL NSE + 5 ng/mL cTnI (I). Error bars = standard deviation (SD) (n = 5).

samples analysis.[36] In detail, α-fetoprotein (AFP), prostate specific antigen (PSA), brain natriuretic peptide (BNP), and cardiac troponin I (cTnI) proteins were chosen as interference substances for investigating the selectivity (Figure 6B). Compared with electrodes a−e which were modified with various interference substances (5 ng/mL) and the detection substance NSE (0.05 ng/mL) only, electrodes f−I were modified with the abovementioned interference substances on the basis of the detection substance NSE. The RSD values of the detection results are less than 5.0%, demonstrating that selectivity of this immunosensor is desirable.

In order to validate the stability, long-term storage of the modified electrodes at 4 °C within 1 month was investigated. The satisfying results are depicted specifically in Figure S8 (Supporting Information).

Analysis of Real Samples. For the purpose of investigating the practical applicability value of the designed split-type EC immunosensor, a standard addition method was applied for NSE analysis throughout this research. The NSE sample in normal human serum samples (diluted with pH 7.4 PBS buffer solution) spiked with 0.05, 0.1, 0.5, and 5 ng/mL was quantitatively determined by this novel EC immunosensor. Table S1 distinctly illustrates that the RSD was calculated to be 1.8−4.4% together with acceptable recoveries ranging from 99.7 to 102.2% (n = 5). In view of the above results, powerful evidence was provided to realize its potential applications for accurate assay of NSE and even other biomarkers.

CONCLUSIONS

To sum up, a split-type EC immunosensor separating the immunoreaction process from EC detection has been fabricated on basis of the controlled-release strategy. Thus, mutual interference between the biometric and EC detection systems was minimized and complexity of the analysis system was further reduced. The SBG_{CdS}−AA conjugate acted as the signal amplifier that encapsulated the AA molecule in the SBG nanocarrier with the CdS cap. Subsequently, oxidation of the released AA was synergistically catalyzed by Fc and GNPs, which immobilized on the p-BVO substrate (FcAI/L-Cys/GNPs/p-BVO/ITO) to trigger the AA-mediated significant signal magnification in this work. Strikingly, the designed immunosensor features admirable sensitivity that could originate from the accelerated electron transfer along the ordered array structure of the p-BVO substrate. Meanwhile, using NSE as the sample biomarker, this versatile system provided a satisfactory linear range together with a low LOD that verified its potential in trace biomarker analysis. This novel EC immunosensor broadened the application of the controlled-release strategy in the field of biosensing.

ASSOCIATED CONTENT

Supporting Information

The Supporting Information is available free of charge at https://pubs.acs.org/doi/10.1021/acsami.1c07780.

Reagents and chemicals; apparatus; additional material preparation process; characterization of materials including XPS spectral data, BET, and FTIR absorption curve, TEM mapping images; p-BVO NA electroactive surface area determination; and additional EC experimental details (PDF)

AUTHOR INFORMATION

Corresponding Author

Qin Wei − *Collaborative Innovation Center for Green Chemical Manufacturing and Accurate Detection, Key Laboratory of Interfacial Reaction & Sensing Analysis in Universities of Shandong, School of Chemistry and Chemical Engineering, University of Jinan, Jinan 250022, Shandong, China*; orcid.org/0000-0002-3034-8046; Email: sdjndxwq@163.com

Authors

Liu Qu − *Collaborative Innovation Center for Green Chemical Manufacturing and Accurate Detection, Key Laboratory of Interfacial Reaction & Sensing Analysis in Universities of Shandong, School of Chemistry and Chemical Engineering, University of Jinan, Jinan 250022, Shandong, China*

Xiang Ren − *Collaborative Innovation Center for Green Chemical Manufacturing and Accurate Detection, Key Laboratory of Interfacial Reaction & Sensing Analysis in Universities of Shandong, School of Chemistry and Chemical Engineering, University of Jinan, Jinan 250022, Shandong, China*; orcid.org/0000-0002-4321-4282

Dawei Fan − *Collaborative Innovation Center for Green Chemical Manufacturing and Accurate Detection, Key Laboratory of Interfacial Reaction & Sensing Analysis in Universities of Shandong, School of Chemistry and Chemical Engineering, University of Jinan, Jinan 250022, Shandong, China*

Xuan Kuang − *Collaborative Innovation Center for Green Chemical Manufacturing and Accurate Detection, Key Laboratory of Interfacial Reaction & Sensing Analysis in Universities of Shandong, School of Chemistry and Chemical Engineering, University of Jinan, Jinan 250022, Shandong, China*; orcid.org/0000-0003-0310-6620

Xu Sun − *Collaborative Innovation Center for Green Chemical Manufacturing and Accurate Detection, Key Laboratory of Interfacial Reaction & Sensing Analysis in Universities of Shandong, School of Chemistry and Chemical Engineering, University of Jinan, Jinan 250022, Shandong, China*; orcid.org/0000-0001-8762-4243

Bin Wang − *Collaborative Innovation Center for Green Chemical Manufacturing and Accurate Detection, Key Laboratory of Interfacial Reaction & Sensing Analysis in Universities of Shandong, School of Chemistry and Chemical Engineering, University of Jinan, Jinan 250022, Shandong, China*; orcid.org/0000-0002-7331-2959

Huangxian Ju − *Collaborative Innovation Center for Green Chemical Manufacturing and Accurate Detection, Key Laboratory of Interfacial Reaction & Sensing Analysis in Universities of Shandong, School of Chemistry and Chemical Engineering, University of Jinan, Jinan 250022, Shandong, China;* orcid.org/0000-0002-6741-5302

Complete contact information is available at: https://pubs.acs.org/10.1021/acsami.1c07780

Notes

The authors declare no competing financial interest.

■ ACKNOWLEDGMENTS

This study was supported by the National Key Scientific Instrument and Equipment Development Project of China (no. 21627809), the National Natural Science Foundation of China (nos. 21777056), the Special Foundation for Taishan Scholar Professorship of Shandong Province, the Jinan Scientific Research Leader Workshop Project (2018GXRC024, 2018GXRC021), and the Innovation Team Project of Colleges and Universities in Jinan (no. 2019GXRC027).

■ REFERENCES

(1) Ma, N.; Ren, X.; Wang, H.; Kuang, X.; Fan, D.; Wu, D.; Wei, Q. Ultrasensitive Controlled Release Aptasensor Using Thymine-Hg^{2+}-Thymine Mismatch as a Molecular Switch for Hg^{2+} Detection. *Anal. Chem.* **2020**, *92*, 14069−14075.

(2) Eissa, S.; Zourob, M. Development of a Low-Cost Cotton-Tipped Electrochemical Immunosensor for the Detection of SARS-CoV-2. *Anal. Chem.* **2021**, *93*, 1826−1833.

(3) Yang, L.; Yin, X.; An, B.; Li, F. Precise Capture and Direct Quantification of Tumor Exosomes via a Highly Efficient Dual-Aptamer Recognition-Assisted Ratiometric Immobilization-Free Electrochemical Strategy. *Anal. Chem.* **2021**, *93*, 1709−1716.

(4) Li, C.; Cui, Y.; Ren, J.; Zou, J.; Kuang, W.; Sun, X.; Hu, X.; Yan, Y.; Ling, X. Novel Cells-Based Electrochemical Sensor for Investigating the Interactions of Cancer Cells with Molecules and Screening Multitarget Anticancer Drugs. *Anal. Chem.* **2021**, *93*, 1480−1488.

(5) Li, Y.; Liu, L.; Liu, X.; Ren, Y.; Xu, K.; Zhang, N.; Sun, X.; Yang, X.; Ren, X.; Wei, Q. A Dual-Mode PCT Eectrochemical Immunosensor with $CuCo_2S_4$ Bimetallic Sulfides as Enhancer. *Biosens. Bioelectron.* **2020**, *163*, 112280.

(6) Cao, L.; Cai, J.; Deng, W.; Tan, Y.; Xie, Q. $NiCoO_2$@CeO_2 Nanoboxes for Ultrasensitive Electrochemical Immunosensing Based on the Oxygen Evolution Reaction in a Neutral Medium: Application for Interleukin-6 Detection. *Anal. Chem.* **2020**, *92*, 16267−16273.

(7) Hu, Q.; Gan, S.; Bao, Y.; Zhang, Y.; Han, D.; Niu, L. Electrochemically Controlled ATRP for Cleavage-Based Electrochemical Detection of the Prostate-Specific Antigen at Femtomolar Level Concentrations. *Anal. Chem.* **2020**, *92*, 15982−15988.

(8) Xue, J.; Jia, Y.; Yang, L.; Feng, J.; Wu, D.; Ren, X.; Du, Y.; Ju, H.; Wei, Q. Etching Triangular Silver Nanoparticles by Self-generated Hydrogen Peroxide to Initiate the Response of an Electrochemiluminescence Sensing Platform. *Anal. Chem.* **2020**, *92*, 14203−14209.

(9) Cao, J.-T.; Wang, B.; Dong, Y.-X.; Wang, Q.; Ren, S.-W.; Liu, Y.-M.; Zhao, W.-W. Photogenerated Hole-Induced Chemical Redox Cycling on Bi_2S_3/$Bi_2Sn_2O_7$ Heterojunction: Toward General Amplified Split-Type Photoelectrochemical Immunoassay. *ACS Sens.* **2018**, *3*, 1087−1092.

(10) Li, X.; Wang, X.; Zhang, L.; Gong, J. High-Throughput Signal-On Photoelectrochemical Immunoassay of Lysozyme Based on Hole-Trapping Triggered by Disintegrating Bioconjugates of Dopamine-Grafted Silica Nanospheres. *ACS Sens.* **2018**, *3*, 1480−1488.

(11) Zhang, S.; Yang, Y.; Tong, Z.; Gao, B.; Gao, N.; Shen, T.; Wan, Y.; Yu, Z.; Liu, L.; Ma, X.; Guo, Y.; Fugice, J.; Li, Y. C. Self-Assembly of Hydrophobic and Self-Healing Bionanocomposite-Coated Controlled-Release Fertilizers. *ACS Appl. Mater. Interfaces* **2020**, *12*, 27598−27606.

(12) Leng, D.; Li, J.; Xu, R.; Liu, L.; Liu, X.; Fan, D.; Wang, H.; Wei, Q.; Ju, H. THCH as Electron Donor in Controlled-Release System for Procalcitonin Analysis Based on $Bi_2Sn_2O_7$ Photoanode. *Sens. Actuators, B* **2020**, *321*, 128509.

(13) Wang, W.; Li, X.; Tang, K.; Song, Z.; Luo, X. A AuNP-capped Cage Fluorescent Biosensor Based on Controlled-release and Cyclic Enzymatic Amplification for Ultrasensitive Detection of ATP. *J. Mater. Chem. B* **2020**, *8*, 5945−5951.

(14) Xu, R.; Liu, L.; Liu, X.; Li, Y.; Feng, R.; Wang, H.; Fan, D.; Wu, D.; Wei, Q. Novel Electron Donor Encapsulation Assay Based on the Split-type Photoelectrochemical Interface. *ACS Appl. Mater. Interfaces* **2020**, *12*, 7366−7371.

(15) Liang, Q.; Hu, Q.; Miao, G.; Yuan, B.; Chen, X. A Facile Synthesis of Novel Mesoporous Bioactive Glass Nanoparticles with Various Morphologies and Tunable Mesostructure by Sacrificial Liquid Template Method. *Mater. Lett.* **2015**, *148*, 45−49.

(16) Luz, G. M.; Mano, J. F. Nanoengineering of Bioactive Glasses: Hollow and Dense Nanospheres. *J. Nanoparticle Res.* **2013**, *15*, 1457.

(17) El-Fiqi, A.; Kim, T.-H.; Kim, M.; Eltohamy, M.; Won, J.-E.; Lee, E.-J.; Kim, H.-W. Capacity of Mesoporous Bioactive Glass Nanoparticles to Deliver Therapeutic Molecules. *Nanoscale* **2012**, *4*, 7475−7488.

(18) Lai, C.-Y.; Trewyn, B. G.; Jeftinija, D. M.; Jeftinija, K.; Xu, S.; Jeftinija, S.; Lin, V. S.-Y. A Mesoporous Silica Nanosphere-Based Carrier System with Chemically Removable CdS Nanoparticle Caps for Stimuli-Responsive Controlled Release of Neurotransmitters and Drug Molecules. *J. Am. Chem. Soc.* **2003**, *125*, 4451−4459.

(19) Wang, J.-Y.; Chen, L.-C.; Ho, K.-C. Synthesis of Redox Polymer Nanobeads and Nanocomposites for Glucose Biosensors. *ACS Appl. Mater. Interfaces* **2013**, *5*, 7852−7861.

(20) Shen, W.-J.; Zhuo, Y.; Chai, Y.-Q.; Yang, Z.-H.; Han, J.; Yuan, R. Enzyme-Free Electrochemical Immunosensor Based on Host-Guest Nanonets Catalyzing Amplification for Procalcitonin Detection. *ACS Appl. Mater. Interfaces* **2015**, *7*, 4127−4134.

(21) Walsh, M. J.; Yoshida, K.; Kuwabara, A.; Pay, M. L.; Gai, P. L.; Boyes, E. D. On the Structural Origin of the Catalytic Properties of Inherently Strained Ultrasmall Decahedral Gold Nanoparticles. *Nano Lett.* **2012**, *12*, 2027−2031.

(22) Gu, H.; Yang, Y.; Tian, J.; Shi, G. Photochemical Synthesis of Noble Metal (Ag, Pd, Au, Pt) on Graphene/ZnO Multihybrid Nanoarchitectures as Electrocatalysis for H_2O_2 Reduction. *ACS Appl. Mater. Interfaces* **2013**, *5*, 6762−6768.

(23) Fang, B.; Deng, X. H.; Kan, X. W.; Tao, H. S.; Zhang, W. Z.; Li, M. G. Electrochemical and Electrocatalytic Properties of Ferrocene Incorporated inL-Cysteine Self-Assembled Monolayers on a Gold Electrode. *Anal. Lett.* **2006**, *39*, 697−707.

(24) Li, Y.; Xuan, J.; Song, Y.; Qi, W.; He, B.; Wang, P.; Qin, L. Nanoporous Glass Integrated in Volumetric Bar-Chart Chip for Point-of-Care Diagnostics of Non-Small Cell Lung Cancer. *ACS Nano* **2016**, *10*, 1640−1647.

(25) Naito, A.; Taguchi, S.; Nakagawa, T.; Matsumoto, A.; Nagase, Y.; Tabata, M.; Miyakawa, J.; Suzuki, M.; Nishimatsu, H.; Enomoto, Y.; Takahashi, S.; Okaneya, T.; Yamada, D.; Tachikawa, T.; Minowada, S.; Fujimura, T.; Fukuhara, H.; Kume, H.; Homma, Y. Prognostic significance of serum neuron-specific enolase in small cell carcinoma of the urinary bladder. *World J. Urol.* **2017**, *35*, 97−103.

(26) Fan, Y.; Liu, J.; Wang, Y.; Luo, J.; Xu, H.; Xu, S.; Cai, X. A Wireless Point-of-Care Testing System for the Detection of Neuron-Specific Enolase with Microfluidic Paper-Based Analytical Devices. *Biosens. Bioelectron.* **2017**, *95*, 60−66.

(27) Feng, J.; Li, F.; Liu, L.; Liu, X.; Qian, Y.; Ren, X.; Wang, X.; Wei, Q. Ultrasensitive Photoelectrochemical Immunosensor for Procalcitonin Detection with Porous Nanoarray $BiVO_4$/Cu_xS Plat-

form as Advanced Signal Amplification under Anodic Bias. *Sens. Actuators, B* **2020**, *308*, 127685.
(28) Qian, Y.; Feng, J.; Xu, R.; Fan, D.; Du, Y.; Ren, X.; Wei, Q.; Ju, H. Zinc and Molybdenum Co-Doped BiVO4 Nanoarray for Photoelectrochemical Diethylstilbestrol Analysis Based on the Dual-Competitive System of Manganese Hexacyanoferrate Hydrate Nanocubes. *ACS Appl. Mater. Interfaces* **2020**, *12*, 16662−16669.
(29) An, Y.; Li, R.; Zhang, F.; He, P. Magneto-Mediated Electrochemical Sensor for Simultaneous Analysis of Breast Cancer Exosomal Proteins. *Anal. Chem.* **2020**, *92*, 5404−5410.
(30) Wang, J.; Li, W.; Lu, Z.; Zhang, L.; Hu, Y.; Li, Q.; Du, W.; Feng, X.; Jia, H.; Liu, B.-F. The Use of RGD-engineered Exosomes for Enhanced Targeting Ability and Synergistic Therapy toward Angiogenesis. *Nanoscale* **2017**, *9*, 15598−15605.
(31) Zhu, Y.; Liu, X.; Yan, K.; Zhang, J. A Cathodic Photovoltammetric Sensor for Chloramphenicol Based on BiOI and Graphene Nanocomposites. *Sens. Actuators, B* **2019**, *284*, 505−513.
(32) Wang, M.; Wang, Q.; Guo, P.; Jiao, Z. In Situ Fabrication of Nanoporous $BiVO_4/Bi_2S_3$ Nanosheets for Enhanced Photoelectrochemical Water Splitting. *J. Colloid Interface Sci.* **2019**, *534*, 338−342.
(33) Qu, L.; Yang, L.; Li, Y.; Ren, X.; Wang, H.; Fan, D.; Wang, X.; Wei, Q.; Ju, H. Dual-Signaling Electrochemical Ratiometric Method for Competitive Immunoassay of CYFRA21-1 Based on Urchin-like Fe_3O_4@PDA-Ag and $Ni_3Si_2O_5(OH)_4$-Au Absorbed Methylene Blue Nanotubes. *ACS Appl. Mater. Interfaces* **2021**, *13*, 5795−5802.
(34) Yang, L.; Jia, Y.; Wu, D.; Zhang, Y.; Ju, H.; Du, Y.; Ma, H.; Wei, Q. Synthesis and Application of CeO_2/SnS_2 Heterostructures as a Highly Efficient Coreaction Accelerator in the Luminol-Dissolved O_2 System for Ultrasensitive Biomarkers Immunoassay. *Anal. Chem.* **2019**, *91*, 14066−14073.
(35) Chen, P.; Qiao, X.; Liu, J.; Xia, F.; Tian, D.; Zhou, C. Dual-Signaling Amplification Electrochemical Aptasensor Based on Hollow Polymeric Nanospheres for Acetamiprid Detection. *ACS Appl. Mater. Interfaces* **2019**, *11*, 14560−14566.
(36) Qu, L.; Yang, L.; Ren, Y.; Ren, X.; Fan, D.; Xu, K.; Wang, H.; Li, Y.; Ju, H.; Wei, Q. A signal-off electrochemical sensing platform based on Fe3S4-Pd and pineal mesoporous bioactive glass for procalcitonin detection. *Sens. Actuators, B* **2020**, *320*, 128324.

https://doi.org/10.1021/acsami.1c07780
ACS Appl. Mater. Interfaces 2021, 13, 29179−29186